Available online at www.sciencedirect.com

ScienceDirect

Scripta Materialia 81 (2014) 32–35

Scripta MATERIALIA

www.elsevier.com/locate/scriptamat

Discovery of a meta-stable Al–Sm phase with unknown stoichiometry using a genetic algorithm

Feng Zhang,* Ian McBrearty, R.T. Ott, E. Park, Mikhail I. Mendelev, M.J. Kramer, Cai-Zhuang Wang and Kai-Ming Ho

Ames Laboratory, US Department of Energy, Iowa State University, Ames, IA 50011, USA

Received 24 January 2014; revised 25 February 2014; accepted 25 February 2014
Available online 6 March 2014

Unknown crystalline phases observed during the devitrification process of glassy metal alloys significantly limit our ability to understand and control phase selection in these systems driven far from equilibrium. Here, we report a new meta-stable Al_5Sm phase identified by simultaneously searching Al-rich compositions of the Al–Sm system, using an efficient genetic algorithm. The excellent match between calculated and experimental X-ray diffraction patterns confirms that this new phase appeared in the crystallization of melt-spun $Al_{90}Sm_{10}$ alloys.
Published by Elsevier Ltd. on behalf of Acta Materialia Inc.

Keywords: Bulk metallic glass; Melt spinning; X-ray diffraction; First-principles calculation; Genetic algorithm

Al alloyed with 10 at.% Sm typifies a class of amorphous materials made by aluminum and rare earth (RE) metals that display attractive mechanical properties [1–3]. When as-quenched amorphous $Al_{90}Sm_{10}$ alloys are isochronally heated, they show a multi-step devitrification pathway that involves a number of meta-stable crystalline phases, as identified by X-ray diffraction (XRD) measurements [4,5]. We have revisited the phase selection in Al–RE alloys produced by melt spinning. By using higher resolution in situ time-resolved XRD at Advanced Photon Source (APS) we can better separate out the individual phases during devitrification. In the past these have been identified as M1, MS1, M2, etc. [4,5]. Understanding the atomic structures of these phases is a prerequisite for answering intriguing questions regarding what controls the complicated phase selection during amorphization or devitrification processes. However, solving these structures has proven to be a challenging task in over a decade after their first detection. An important reason for these difficulties is the unknown stoichiometries of these phases, which significantly complicates structure determination either by direct XRD measurements or by searching the configurational space with a global optimization method.

In this paper, we search for these meta-stable crystalline phases using a genetic algorithm (GA) that was originally proposed to solve cluster structures [6], and later successfully demonstrated in predicting crystal structures [7–10]. Here, we include a variation of this method that enables simultaneous determination of low-energy structures for a wide range of compositions and unit-cell sizes, using a method similar to that outlined in Ref. [11]. That is, in each generation of the "genetic evolution", structures with different compositions and unit-cell sizes are allowed to coexist in the pool. The fitness for each structure is defined as its distance from the convex hull of the pool in the energy vs. composition plot, as schematically illustrated in Fig. 1. "Parent" structures are selected primarily from those with low fitness values to create offspring structures based on the "mating" operations introduced in Ref. [6,7]. In previous applications, additional steps had to be taken in order to fix the composition and unit-cell size. Here, we skip these steps to ensure the diversity of compositions and unit-cell sizes in the next generation. The structures with high fitness values will be replaced by the offspring structures that have lower

* Corresponding author. Tel.: +1 5152946878; e-mail addresses: fzhang@ameslab.gov; kmh@ameslab.gov

http://dx.doi.org/10.1016/j.scriptamat.2014.02.019
1359-6462/Published by Elsevier Ltd. on behalf of Acta Materialia Inc.

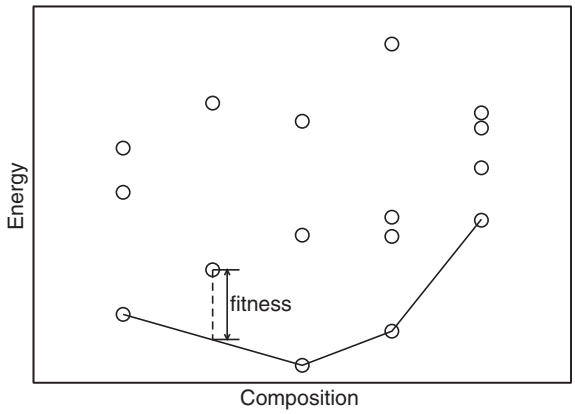

Fig. 1. Schematic of the definition of the fitness of a structure used in the GA search. Each circle represents a structure in the pool. The solid line forms the convex hull of all the structures.

fitness values. The above steps are repeated until the structure pool stops evolving.

To facilitate the GA search, we use a classical interatomic potential in the Finnis–Sinclair (FS) format [12] for energy calculations. Fig. 2(a) plots the formation energy (E_{form}) at zero temperature calculated by the FS potential, for the known stable and meta-stable Al–Sm phases with various Al composition (x_{Al}). E_{form} for an intermetallic phase $\text{Al}_x\text{Sm}_{1-x}$ is defined as:

$$E_{\text{form}}(\text{Al}_x\text{Sm}_{1-x}) = E(\text{Al}_x\text{Sm}_{1-x}) - xE(\text{Al}) - (1-x)E(\text{Sm}), \quad (1)$$

where $E(\text{Al}_x\text{Sm}_{1-x}), E(\text{Al})$ and $E(\text{Sm})$ denote the total energy per atom for $\text{Al}_x\text{Sm}_{1-x}$, fcc Al and trigonal Sm, respectively. In Fig. 2(a), the solid line connects the phases that are thermodynamic stable at low temperatures in the Al–Sm phase diagram [13]. The remaining are theree meta-stable phases that have already been identified in experiments, including the orthorhombic $\text{Al}_{11}\text{Sm}_3$ (o-$\text{Al}_{11}\text{Sm}_3$), the orthorhombic Al_4Sm (o-Al_4Sm) and the tetragonal Al_4Sm (t-Al_4Sm). If the calculations are reliable, the stable phases should form the convex hull for all the phases. As seen from Fig. 2(a), except that the stability of AlSm_2 is slightly underestimated, and the stability of o-$\text{Al}_{11}\text{Sm}_3$ and o-Al_4Sm is slightly overestimated, the FS potential in general gives a satisfactory estimation of the relative thermodynamic stability of the known stable and meta-stable phases. It is therefore reasonable to use this FS potential to calculate the energy for the first round of screening. After the GA search is converged, the best structures found in the converged pool are then selected for more accurate calculations using the density-functional theory (DFT), as implemented within the VASP package [14,15]. The generalized gradient approximation proposed by Perdew, Burke, and Ernzerhof [16] is used for the exchange–correlation functional. The electron–ion interaction is treated with the projector-augmented wave method [17]. A cut-off energy of 400 eV is used for the plane-wave basis. The total-energy converges to 10^{-5} eV per cell in each self-consistent loop, and the structural relaxation terminates when the force on each atom is smaller than 0.01 eV Å^{-1}.

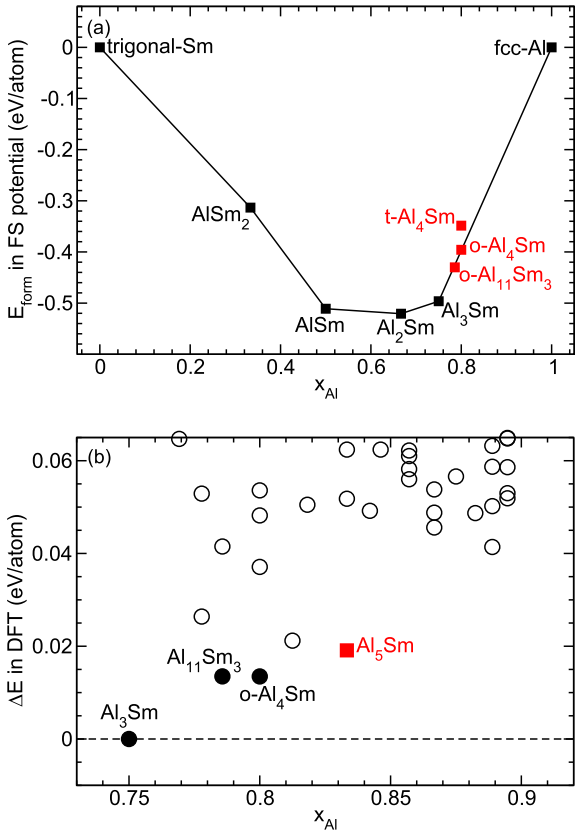

Fig. 2. (a) The formation energy of known stable and meta-stable phases at $T = 0$ calculated by the FS potential, as a function of the Al composition. The solid line connects the thermodynamically stable phases (black squares) shown in the phase diagram. The red squares denote three meta-stable phases at low temperatures. (b) The driving force for phase separation into the equilibrium mixture of Al_3Sm and Al for low-energy structures found in the GA search, as a function of the Al composition. The solid black circles denote the phases that are previously known. The red square denotes the newly found Al_5Sm phase. The dashed line denotes the tie line connecting the Al_3Sm phase and the pure Al. (For interpretation of the references to colour in this figure legend, the reader is referred to the web version of this article.)

Although the stoichiometries of the meta-stable phases that appear during the devitrification of glassy $\text{Al}_{90}\text{Sm}_{10}$ alloys are unknown, it is reasonable to assume that they all contain higher Al content than the hexagonal Al_3Sm phase ($x_{\text{Al}} = 0.75$), which is the stable Al–Sm compound with the highest Al composition in the Al–Sm phase diagram [13]. This assumption is based on the fact the unknown phases were observed in the crystallization of amorphous Al–Sm with x_{Al} as high as 90%. Thus, we use 0.75 and 0.9 as lower and upper bounds for x_{Al} in our GA search, respectively.

Fig. 2(b) shows the structures with relatively low fitness values found by a GA search performed with constraints $0.75 \leqslant x_{\text{Al}} \leqslant 0.9$ and $N \leq 20$ (N is the number of atoms in a unit cell). All the structures shown in Fig. 2 (b) are fully relaxed by DFT. To measure the stability of these phases, we define ΔE, the driving force for decomposing into the equilibrium mixture of Al and Al_3Sm, as:

$$\Delta E(\text{Al}_x\text{Sm}_{1-x}) = E(\text{Al}_x\text{Sm}_{1-x}) - (4x-3)E(\text{Al}) - (1-x)E(\text{Al}_3\text{Sm}). \quad (2)$$

Previously known compounds in the composition range $0.75 \leqslant x_{Al} \leq 0.9$ are all recovered in the GA search. The Al_3Sm, o-$Al_{11}Sm_3$, and o-Al_4Sm are denoted as black solid circles in Fig. 2(b). The t-Al_4Sm phase is not shown in Fig. 2 (b) due to its high ΔE of 0.10 eV/atom.

In addition, the final pool contains a lot of new structures with a wide range of compositions. These phases are compared with in situ high temperature X-ray diffraction patterns collected at the Advance Photon Source at Argonne National Laboratory at beamline 1-ID-D. Melt spun amorphous ribbons Al-10 at.% Sm were sealed in thin walled capillary tubes in Ar and heated at 10 K/min from 300 to 773 K. The scattering was performed in a transmission geometry with 4 GE area detectors positioned at 2078.28 mm from the sample using high energy monochromatic X-rays with $\lambda = 0.1536$ Å. We acquired diffraction data every 6 s using four detectors. The large area covered by the 4 detectors and their distance from the sample provide very high reciprocal space resolution (0.014 $Å^{-1}$), high signal to noise ratio, and a large reciprocal range for accurate Rietveld fitting. The fine time resolution of the XRD, 1 pattern per degree K, resulted in a one-to-one correspondence to the exothermic events observed in the differential scanning calorimeter (DSC), that is, from glass to a cubic MS1 phase at 465 K, and from MS1 to a mixture of $Al_{11}Sm_3$, fcc Al, and another unknown M1 phase at 527 K. The M1 phase continues to grow and increases in phase proportion, comprising 54 wt.% of the sample by ~650 K. Above this temperature the M1 phase decomposes. We choose to fit the data at 626 K in the Rietveld refinement, which is in the middle of the stability range for the M1.

From the Rietveld refinement, we found that a hexagonal phase with the stoichiometry Al_5Sm and space group P6/mmm (No. 191), denoted as the red square in Fig. 2(b), matches well with the meta-stable M1 phase that appeared in the crystallization of the melt-spun $Al_{90}Sm_{10}$ sample at 626 K [see Fig. 3(a)]. The XRD pattern in Fig. 3(a) is comprised of three different phases: the tetragonal $Al_{11}Sm_3$ (t-$Al_{11}Sm_3$), fcc Al and Al_5Sm, which constitute ~10, 40 and 50 wt.%, respectively. The excellent match between the experimental and calculated XRD patterns ($wR_p = 3.8\%$) confirms our prediction of the Al_5Sm phase. Table 1 shows the lattice parameters and the atomic coordinates of the Al_5Sm phase, given by both DFT calculations and the Rietveld analysis, which further confirms our prediction is highly accurate. Fig. 3 (b) gives the atomic structure of Al_5Sm, which successively contains a hexagonal Al layer, a triangular Sm layer, a second hexagonal Al layer, and a triangular Al layer, along the *c*-axis. In Fig. 3(c), a cluster formed by a central Sm and surrounding Al atoms in the Al_5Sm phase is shown. It has a shape of a hexagonal prism capped by a hexagonal pyramid on both ends.

At $T = 0$, the Al_5Sm phase is 0.019 eV/atom unstable with respect to phase separation into the Al_3Sm phase and pure Al, as shown by the ΔE value of this structure in Fig. 2 (b). To investigate the effects of finite temperatures, we have included the vibrational free energy F_{vib} by performing phonon calculations. Fig. 4(a) shows the phonon density of states for the Al_5Sm phase. No

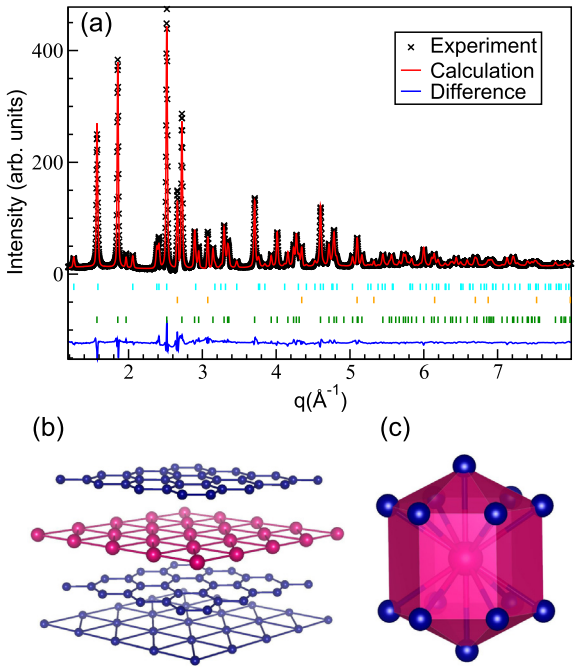

Fig. 3. (a) Rietveld fitting of the XRD patterns for melt-spun $Al_{90}Sm_{10}$ sample at 626 K, showing the crystallization products of tetragonal $Al_{11}Sm_3$, fcc Al, and the newly found hexagonal Al_5Sm. The vertical lines in light blue, brown, and green show the diffraction peak positions for tetragonal $Al_{11}Sm_3$, Al, and Al_5Sm, respectively. (b) Layer-by-layer structure of Al_5Sm. The inter-layer bonds are not shown for easier viewing. (c) Sm-centered cluster in Al_5Sm. Blue (red) represents Al (Sm) atoms. (For interpretation of the references to colour in this figure legend, the reader is referred to the web version of this article.)

imaginary phonon modes are observed, indicating that the Al_5Sm is dynamically stable. Under the harmonic approximation, F_{vib} takes the form

$$F_{vib} = k_B T \sum_{nk} \ln\left[2\sinh\frac{\hbar\omega_n(k)}{2k_B T}\right], \quad (3)$$

where $\omega_n(k)$ represents the phonon dispersion relation. Then, the free energy difference between the Al_5Sm phase and the phase-separated mixture of Al_3Sm and pure Al can be calculated as

$$\Delta F = \Delta E + \Delta F_{vib}. \quad (4)$$

In Fig. 4(b), we plot ΔF as a function of the tempearture. Although ΔF decreases with T, it remains positive for a temperature as high as 1300 K. This indicates that Al_5Sm is only meta-stable for the entire solid temperature range.

None of the other meta-stable phases shown in Fig. 2(b) match the unknown phases detected in XRD measurements. Other GA searches with maximal unit cell sizes as large as 50 atoms/unit cell did not identify any new phases either. Of course, since difficulty of searching the configurational space increases exponentially with the size of the system, it is possible that the GA search for large systems failed to converge. However, another possibility is that the other phases involve disordered vacancies or antisite defects associated with partial occupancies of certain Wyckoff positions. Such

Table 1. Lattice parameters and atomic coordinates of the Al_5Sm phase with the space group P6/mmm. The numbers in parentheses are given by Rietveld analysis, and the rest by DFT calculations.

Lattice parameters (in units of Å).			
$a = 4.597$ (4.957)	$c = 6.356$ (6.358)		
	Atomic coordinates		
	x	y	z
Al1	0	0	0
Al2	1/3	2/3	0.214 (0.217)
Sm1	0	0	0.5

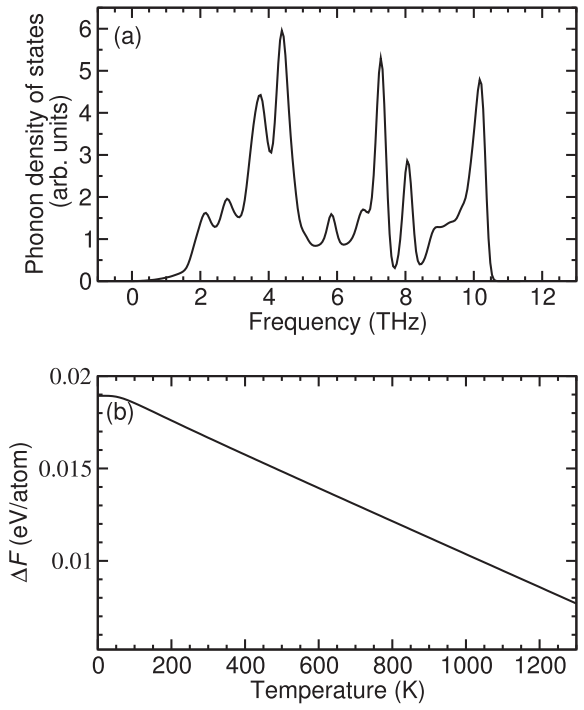

Fig. 4. (a) Phonon density of states of the Al_5Sm phase. (b) ΔF calculated according to Eq. 4 as a function of the temperature.

phenomenon is commonly seen in intermetallics. An example is the t-$Al_{11}Sm_3$ phase, which is derived from the t-Al_4Sm phase by introducing disordered Al vacancies. New methodologies to meet this challenge is still highly desirable in theoretical structure prediction.

In summary, we simultaneously search a wide range of Al-rich stoichiometries for unknown meta-stable phases observed during the devitrification of Al–Sm glasses, using an efficient genetic algorithm. We successfully recovered all previously known compounds in the studied composition range. More importantly, we found a new phase with the stoichiometry Al_5Sm. The calculated X-ray diffraction spectrum matches excellently with that of the experiments. Al_5Sm is meta-stable with respect to phase separation into Al_3Sm and pure Al at finite temperatures. The application of this combined experimental and computational approach has implications for understanding and controlling phase selection in highly-driven systems.

Work at Ames Laboratory was supported by the US Department of Energy, Basic Energy Sciences, Division of Materials Science and Engineering, under Contract No. DE-AC02-07CH11358, including a grant of computer time at the National Energy Research Supercomputing Center (NERSC) in Berkeley, CA. The high-energy X-ray experiments were performed at the XOR beamline (sector 1) of the Advanced Photon Source, Argonne National Laboratory, under Grant No. DE-AC02-06CH11357. We would like to thank Jon Almer for his assistance in setting up these experiments.

[1] Y. He, S.J. Poon, G.J. Shiflet, Science 241 (1988) 1640.
[2] Z.C. Zhong, X.Y. Jiang, A.L. Greer, Mater. Sci. Engin. A226 (1997) 531.
[3] A. Inoue, Prog. Mater. Sci. 43 (1998) 365–520.
[4] J.Q. Guo, K. Ohtera, K. Kita, J. Nagohora, N.S. Kazama, Mater. Lett. 24 (1995) 133–138.
[5] P. Rizzi, M. Baricco, S. Borace, L. Battezzati, Mater. Sci. Eng. A A304–306 (2001) 574–578.
[6] D.M. Deaven, K.M. Ho, Phys. Rev. Lett. 75 (1995) 288.
[7] M. Ji, C.Z. Wang, K.M. Ho, Phys. Chem. Chem. Phys. 12 (2010) 11617.
[8] M. Ji, K. Umemoto, C.Z. Wang, K.M. Ho, R.M. Wentzcovitch, Phys. Rev. B 84 (2011) 220105.
[9] S. Wu, K. Umemoto, M. Ji, C.Z. Wang, K.M. Ho, R.M. Wentzcovitch, Phys. Rev. B 83 (2011) 184102.
[10] M.C. Nguyen, J.H. Choi, X. Zhao, C.Z. Wang, Z. Zhang, K.M. Ho, Phys. Rev. Lett. 111 (2013) 165502.
[11] A.R. Oganov, Modern Methods of Crystal Structure Prediction, Wiley-VCH, Singapore, 2011, p. 163.
[12] M.W. Finnis, J.E. Sinclair, Phil. Mag. A 50 (1984) 45.
[13] H. Okamoto, J. Phase Equilibr. Diff. 29 (2008) 200.
[14] G. Kresse, J. Furthmüller, Phys. Rev. B 54 (1996) 11169.
[15] G. Kresse, J. Furthmüller, Comput. Mat. Sci. 6 (1996) 15.
[16] J.P. Perdew, K. Burke, M. Ernzerhof, Phys. Rev. Lett. 77 (1996) 3865, **78**, 1997, 1396.
[17] G. Kresse, J. Hafner, Phys. Rev. B 47 (1993) 558, **49**, 1994, 14251.